A new framework for modeling sediment fining during transport with fragmentation and abrasion

Caroline Le Bouteiller, F. Naaim-Bouvet, N. Mathys, J. Lavé

A new framework for modeling sediment fining during transport with fragmentation and abrasion

C. Le Bouteiller,[1,2] F. Naaim-Bouvet,[1] N. Mathys,[1] and J. Lavé[3]

Received 15 November 2010; revised 15 April 2011; accepted 20 April 2011; published 19 July 2011.

[1] A new framework for modeling sediment fining during transport is proposed. The model is based on a physical description of both abrasion and fragmentation processes. It attempts to describe and explain the changes in the grain-size distribution of sediments during their transport in a water flow. Abrasion and fragmentation are modeled through the use of breakage frequency functions and daughter size distributions. These functions are determined experimentally for the specific case study which is presented. Comparison between the predictions from the model and experimental data from the case study show that (1) both abrasion and fragmentation are involved in the degradation, (2) fragmentation efficiency decreases during the experiment, and (3) the shape of the pebbles provides feedback between abrasion and fragmentation. This type of model is therefore appropriate for explaining degradation mechanisms, which is promising for a future application to rivers.

Citation: Le Bouteiller, C., F. Naaim-Bouvet, N. Mathys, and J. Lavé (2011), A new framework for modeling sediment fining during transport with fragmentation and abrasion, *J. Geophys. Res.*, *116*, F03002, doi:10.1029/2010JF001926.

1. Introduction

[2] A downstream decrease in sediment grain size is often observed in gravel bed rivers [*Kodama*, 1994a; *Brierley and Hickin*, 1985; *Brewer and Lewin*, 1993]. This downstream fining pattern is usually characterized in terms of Sternberg's law [*Sternberg*, 1875], according to which a characteristic grain size D decreases exponentially in the downstream direction. Denoting D_0 the initial grain size, l the traveled distance and β the fining coefficient:

$$D = D_0 e^{-\beta l} \tag{1}$$

[3] β is expressed in m^{-1} and usually referred to as the abrasion coefficient. It represents (at first order) the percentage of reduction of the grain size after traveling a unit distance. A similar law can be inferred for the mass reduction:

$$m = m_0 e^{-\alpha l} \tag{2}$$

[4] α is also expressed in m^{-1}, it represents at first order the percentage of mass that is removed from a grain after traveling a unit distance and it is related to the diameter abrasion coefficient by $\alpha = 3\beta$.

[5] Downstream fining in natural rivers is mainly explained by two processes: selective transport and abrasion [*Parker*, 1991]. Selective transport is due to the fact that small pebbles are likely to be entrained faster and travel further than the bigger ones. Big pebbles deposit preferentially upstream whereas smaller ones are transported downstream, which results in a net fining pattern. Abrasion is due to the friction and collisions that occurs between pebbles and between one pebble and the bed, leading to the size reduction of a pebble. Depending on the concavity of the river and on the bed material lithology, one of these processes might be dominant compared to the other one. For instance, *Frings* [2008] shows that abrasion is negligible compared to selective transport for sand bed rivers. On the other hand, when the lithology is very erodible, abrasion can be the dominant process, such as in Draix alpine catchments, that are located on a marly substratum [*Le Bouteiller et al.*, 2009]. In this paper, the analysis is focused on abrasion fining processes.

[6] The word "abrasion" (in its broad meaning) actually refers to the various types of degradation events that lead to the size reduction of a pebble. Kuenen's abrasion classification [*Kuenen*, 1956] distinguishes between seven wearing mechanisms including chipping, crushing, grinding or splitting. Among these, some mechanisms produce very fine particles with little change in the size of the main element, whereas others produce grains of various sizes. Depending on the resulting fragment size distribution, two main types of degradation mechanisms can then be inferred: fragmentation and surface abrasion. In the following, the word "abrasion" will only be used to refer to the latter.

[7] Degradation effects in sediment transport have been studied through the help of various experimental devices, including rotating mills and circular flumes [*Kuenen*, 1956; *Lewin and Brewer*, 2002; *Attal et al.*, 2006; *Kodama*, 1994b]. In all these experiments, a decrease of a characteristic grain

[1]Cemagref ETNA, Grenoble, France.
[2]AgroParistech-Engref, Paris, France.
[3]CRPG-CNRS, Vandoeuvre-lès-Nancy, France.

0148-0227/11/2010JF001926

size as well as a shift of the grain size distribution toward the small sizes is observed, due to either abrasion, fragmentation or both mechanisms. Depending on the loading and on the lithology, one or the other type of degradation is favored. For instance, most of the experiments in small rotating drums fail to represent the fragmentation processes that occur in natural rivers since they do not provide high-energy impacts between particles [*Lewin and Brewer*, 2002]. When both processes are active, integrated experimental measurement of the resulting size distribution does not allow distinguishing between their effects and importance.

[8] Here, a model that takes into account the size reduction effects due to both abrasion and fragmentation is proposed, on the basis of a physical and statistical description of the processes. This type of model has been first proposed by *Parker* [2008] but to our knowledge, has never been applied to a real case study. A physically based model for downstream fining in bedrock stream was proposed by *Chatanantavet et al.* [2008] but in that case, the effects of splitting and fragmentation were only accounted for through the use of a lumped Sternberg's type coefficient. In the present paper, we develop a model that physically describes both abrasion and fragmentation processes. Following the Population Balance Equation (PBE) framework, that has been developed for the chemical industry [*Ramkrishna*, 1985], probability functions are used to describe the breakage frequency and the size distribution of fragments for both abrasion and fragmentation.

[9] The framework used to model the evolution of a grain size distribution subjected to these degradation mechanisms is described in section 2. The model is then applied to a case study, which consists of a circular flume experiment with marly pebbles. This case study is briefly presented in section 3. In order to apply the model, the probability functions for the specific study case are determined using theoretical assumptions as well as experiments, as explained in section 4. Simulation methods are briefly summarized in section 5. The results from the model are presented in section 6, then compared to the experimental data and discussed in section 7.

2. Framework

[10] Consider a natural bed load population, composed of stones of many sizes. Here, the measure used for characterizing the distribution is the mass of the stones x. It can be related to the grain size D which is the diameter of the equivalent sphere of similar mass, so that

$$x = \frac{\pi}{6}\rho D^3 \tag{3}$$

[11] The number density function $f(x,t)$ is defined such that $f(x,t)dx$ denotes the number of grains of mass in the range $[x, x + dx]$ at time t. The zeroth and first moments of the distribution are then the total number of particles $N(t)$ and the mass of the whole population M, respectively.

$$N(t) = \int_0^\infty f(x,t)dx \tag{4}$$

$$M = \int_0^\infty xf(x,t)dx \tag{5}$$

[12] Similarly, it is possible to define the density function $g(r,t)$ based on the particle radius $r = D/2$ by noting that $f(x,t)dx = g(r,t)dr$. Combining this with equation (3) gives

$$g(r,t) = f(x,t)\frac{dx}{dr} = f(x,t)2\pi\rho r^2 = f\left(\frac{4\pi r^3}{3}, t\right)4\pi\rho r^2 \tag{6}$$

[13] Contrary to what is proposed by *Parker* [2008], here the distribution includes not only coarse material but also the fine particles that are produced by abrasion. The total mass M is then conserved and M does not vary with time t.

[14] The evolution of grain mass distribution is described within the population balance equation framework. This framework has been developed and widely used for chemical engineering issues [*Ramkrishna*, 1985; *Iveson et al.*, 2001]. It is based on the description of a population by its size or mass distribution. The various processes that lead to an increase (such as aggregation) or a decrease (such as breakage) in the size of an element of this population are modeled at the individual scale. This number-based framework therefore allows the creation and disappearance of individuals, to determine an evolution of the number of elements in the population.

[15] In our study, size-decreasing processes are the only relevant processes, and we consider a closed system with no input or loss of material. Here we denote $a(x)$ the breakage frequency of particle of mass x, i.e., the probability for a pebble of mass x to break during a duration dt. We also introduce the distribution $p(x,y)$ such that $p(x,y)dx$ is the number of fragments of mass in the range $[x, x + dx]$ created from the breakage of a particle of mass y. The general form of the evolution equation is then the following:

$$\frac{\partial f(x,t)}{\partial t} = -a(x)f(x,t) + \int_x^\infty a(y)p(x,y)f(y,t)dy \tag{7}$$

[16] Equation (7) is a number-based, linear integro-differential equation. $f(x,t)dx$ is the number of grains of mass comprised between x and $x + dx$ at time t, so the left term is the rate of change of f. The first term on the right-hand side of equation (7) denotes the number of former grains of mass x that have been broken during time dt, and the second term accounts for all the new particles of mass x that have been formed by the breakage of bigger particles of mass $y > x$.

[17] In the chemical engineering literature, p is often referred to as the daughter distribution. It satisfies the following relation, where $N_f(y)$ is the average number of fragments for a single breakage event of a particle of mass y:

$$\int_0^\infty p(x,y)dx = N_f(y) \tag{8}$$

In the general case, the average number of fragments may depend on the mass y of the initial particle.

[18] Each breakage event must conserve the mass, which imposes the following condition on p:

$$\int_0^\infty xp(x,y)dx = y \tag{9}$$

[19] This framework has been mostly developed for fragmentation processes but can be adapted to abrasion, so that the two mechanisms could be modeled in a similar way in the present study. In the following, it is assumed that abrasion and fragmentation act separately on the stones. Modeling these two processes separately, as suggested by *Parker* [2008], will allow comparing their effects and efficiency. The possible coupled effects that are neglected here will be discussed in section 7.3. Each of these processes is characterized by its own breakage frequency and daughter distribution, and the PBE can therefore be written:

$$\begin{aligned}\frac{\partial f(x,t)}{\partial t} &= -a_a(x)f(x,t) + \int_x^\infty a_a(y)p_a(x,y)f(y,t)dy \\ &\quad - a_f(x)f(x,t) + \int_x^\infty a_f(y)p_f(x,y)f(y,t)dy\end{aligned} \tag{10}$$

[20] Here the index a refers to the abrasion mechanism, whereas the index f refers to the fragmentation mechanism. The rate of change of f is the difference between the supply from bigger grains that are abraded or fragmented (second and fourth terms) and the loss of particles by abrasion and by fragmentation (first and third terms).

[21] At usual time scales of study, abrasion occurs as a continuous process, therefore the use of a frequency function for abrasion events seems to be an artificial discretization of the abrasion process. However, it is physically justified when looking at smaller time and space scales, where abrasion is actually composed of a succession of discrete events.

[22] Physical investigations on fragmentation have shown that the energy required to damage very small grains tends to the infinity [*Kendall*, 1978]. This principle can be extended similarly for the abrasion mechanism. For that reason, a limit value of mass x_{min} is defined, such that no breakage occurs by either mechanism on particles of mass smaller than x_{min}. The final model can then be written as follows:

$$\begin{aligned}\frac{\partial f(x,t)}{\partial t} &= -a_a(x)f(x,t) - a_f(x)f(x,t) \\ &\quad + \int_x^\infty a_a(y)p_a(x,y)f(y,t)dy \\ &\quad + \int_x^\infty a_f(y)p_f(x,y)f(y,t)dy \text{ for } x > x_{\min} \\ \frac{\partial f(x,t)}{\partial t} &= \int_{x_{\min}}^\infty a_a(y)p_a(x,y)f(y,t)dy \\ &\quad + \int_{x_{\min}}^\infty a_f(y)p_f(x,y)f(y,t)dy \text{ for } x < x_{\min}\end{aligned} \tag{11}$$

[23] In order to apply the model, the four functions a_a, a_f, p_a and p_f need to be determined, as described in section 4. This will be done for the experimental study case described in section 3 with marly pebbles, but a similar methodology can be used to apply the model to any other kind of material.

3. Experimental Study Case

[24] The model is first applied to a degradation experiment that has been performed in a circular flume with marly material. In the experiment, degradation processes due to mechanical loading during transport are the only processes responsible for modifying the grain sizes. The model predictions can therefore be directly compared to experimental measurements of the grain size distribution.

3.1. Material

[25] The material that is used for the experiments comes from the Laval river, which is a small mountainous stream located in the southern Alps in France, in the Draix observatory [*Mathys et al.*, 2003]. The Laval drainage area is mainly composed of marl, a geological formation which is highly erodible and provides large volumes of material to the riverbed. In this catchment, downstream fining patterns [*Le Bouteiller et al.*, 2009] and high concentrations of suspended fine sediment (up to 800 g/L) during floods suggest that the marly sediments are degraded by mechanical loading when transported.

3.2. Experimental Setup

[26] In order to study the degradation of marly material, an annular flume device was used [*Attal et al.*, 2006], as shown in Figure 1. A 14 kg sample of marly pebbles between 8 and 60 mm from the Laval riverbed was introduced in the water flow. For the median grain size that was used (≈30 mm), *Attal and Lavé* [2009] found that, in the flume, the abrasion rate becomes roughly independent of the introduced load mass for a quantity of material larger than 30 kg. For that reason, and in order to maintain approximately constant abrasion rate during experiments despite the large reduction in marly load, 20 kg of quartzite pebbles of sizes 30–40 mm were added to the marly pebbles in the flume. Given the grain size, the total load represents less than one layer of pebbles on the bed. It was independently checked in a smaller flume that the global degradation rate for marl was the same in experiments with only marly pebbles and in experiments with a mixture of marl and quartzite.

[27] In the large flume, the mean fluid velocity was 2.1 m/s, a value that can be commonly reached in the Laval river during floods. For a constant fluid discharge, the mean fluid velocity increases slightly during the experiment (10 to 15%) as the pebbles become smaller. This increase will be neglected in the model. In previous experiments conducted under similar conditions, *Attal and Lavé* [2009] showed that all the grains were in motion and transported mostly in saltation. In addition, these authors used a high-speed camera to develop a calibration for the pebble velocity as a function of the fluid velocity at various loads, sediment sizes and discharges. According to this calibration, the sediment velocity in our experiment is estimated to be 1.2 m/s. The bottom of this flume is made of pieces of tires, which means that the experiment reproduces the interactions between the pebbles but not the interactions between the pebbles and the

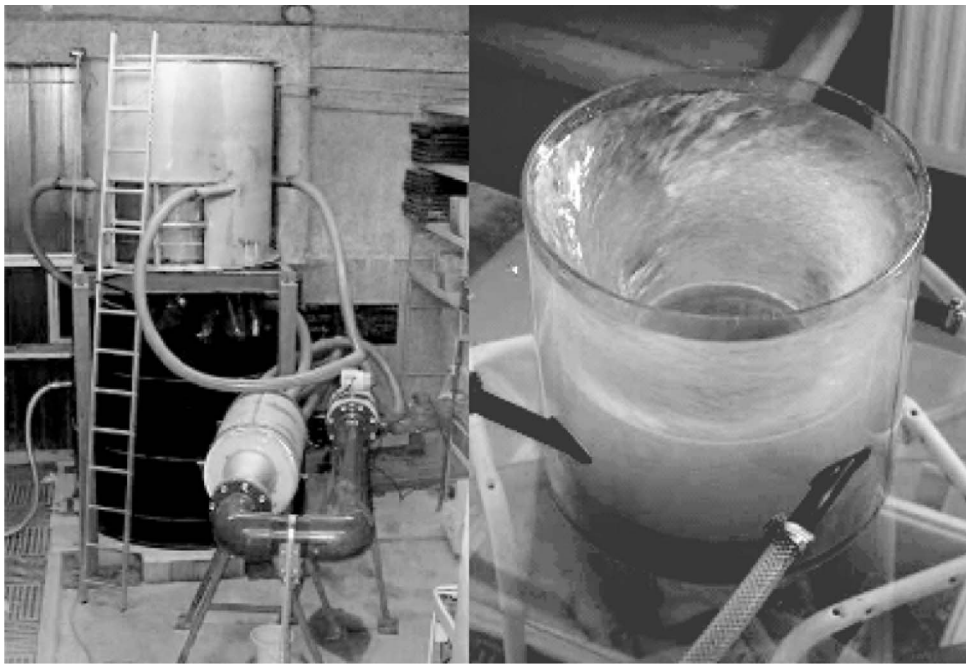

Figure 1. Annular flume devices. (left) Full-scale device. (right) Small-scale device showing the vortex (photos from *Attal and Lavé* [2009]).

bed. In the present paper, the model will be applied to this specific experimental case, but when dealing with natural channels, the interactions with the bed will need to be incorporated.

[28] Every ten minutes, the flow was stopped and the pebbles were removed from the flume for sieving and weighing. Sieves of sizes 5, 8, 10, 15, 20, 32 and 40 mm were used to measure the grain-size distribution. After weighing all the pebbles of size bigger than 5 mm, the mass that was missing was assumed to correspond to particles of size smaller than 5 mm.

3.3. Experimental Results

[29] From qualitative observations, there was evidence of both fragmentation and abrasion, including a production of angular stones, an increase in the number of pebbles and an increase in the concentration of fine particles. The evolution of the cumulative mass distribution is plotted in Figure 2. It shows a clear shift in the distribution toward the smaller sizes. D90 and D50 values interpolated from the distributions are presented in Table 1. The integrated results do not allow a distinction between the effects of abrasion and fragmentation. For instance, the number of particles of size larger than 10 mm is plotted in Figure 3. After the first ten minutes, the increase in the number of pebbles larger than 10 mm shows that there has been some fragmentation. However, the decrease in the number of pebbles larger than 10 mm which occurs after 10 min is more difficult to explain. This decrease can be attributed either to the progressive surface abrasion of pebbles that become smaller than 10 mm, or to the fragmentation of clasts that give birth to particles smaller than 10 mm, or to a combination of both effects. Except from the initial increase that clearly indicates fragmentation, there is no evident distinction between fragmentation and abrasion effects. Applying the model that is proposed in the present paper might therefore help understand better the processes at stake.

4. Function Determination

[30] The model presented in section 2 is based on four elementary functions that describe the frequency of abrasion (a_a) and fragmentation (a_f) and the resulting fragment size distributions for abrasion (p_a) and fragmentation (p_f). The

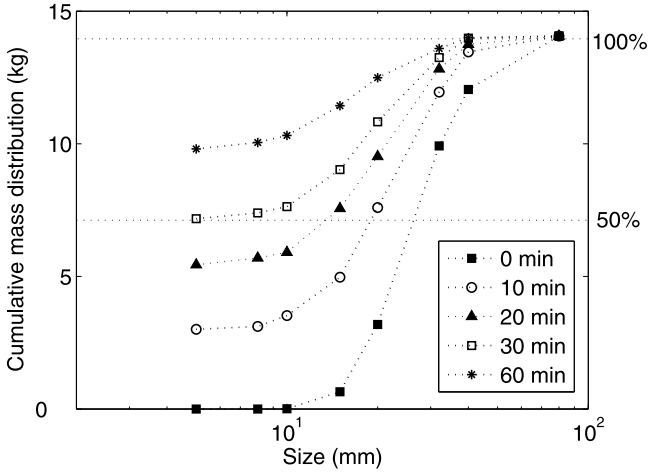

Figure 2. Experimental grain-size distributions for a 1 h experiment. The fraction of the total mass is indicated on the right axis.

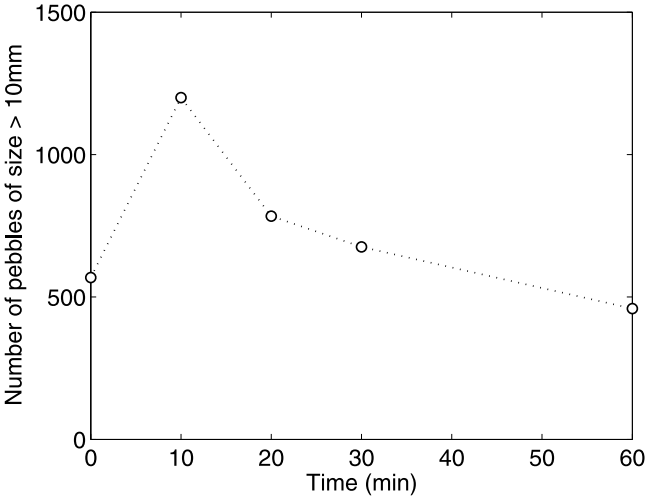

Figure 3. Evolution of the number of particles of size bigger than 10 mm during the experiment.

present section explains how these functions are determined for the specific study case of section 3.

4.1. The Breakage Function for Fragmentation

[31] The breakage frequency a_f is the probability for a pebble of mass x to break during a duration dt. This probability is the product of a collision probability and the conditional breakage probability given the occurrence of a collision.

$$P(Breakage) = P(Collision) \cdot P(Breakage|Collision) \quad (12)$$

[32] In the following, we will first define the probability of collision based on theoretical considerations (see section 4.1.1), then determine the conditional breakage probability using impact experiments (see section 4.1.2).

4.1.1. The Probability of Collision

[33] The probability of a collision is a function of the concentration of particles, of their velocity and of their sizes. The assembly of pebbles in saltation is a dilute granular media where most of the collisions are binary, i.e., only involve two particles, so the framework of the kinetic theory for gasses can be used. Particles are moving at a velocity $u = \bar{u} + \tilde{u}$, where $\bar{u}$ is the mean velocity and $\tilde{u}$ the fluctuations. Here we only consider the velocity in the flow direction and neglect the possible fluctuations in the vertical and radial directions. The average relative velocity between two particles is then of the order of $\langle \tilde{u}^2 \rangle^{1/2}$.

[34] Considering one particle of radius r_1, the number of particles of radius r_2 that are going to impact it during time dt is

$$n_r(r_1, r_2) = \pi (r_1 + r_2)^2 C(r_2) \langle \tilde{u}^2 \rangle^{1/2} dt \quad (13)$$

where $C(r)$ is the concentration (m^{-3}) of particles of radius r in the media, i.e., the number of particles of size r per unit volume. Equation (13) means that during a duration dt, the particle of radius r_1 is going to be impacted by all the particles of radius r_2 that are localized at time t in the cylinder of length $\langle \tilde{u}^2 \rangle^{1/2} dt$ and section $\pi (r_1 + r_2)^2$.

[35] The concentration in the water results from the presence of both marly pebbles and quartzite pebbles in the water. Quartzite is much less sensitive to degradation during transport than marl, its abrasion rate as measured by *Kuenen* [1956] is found to be 0.02%/km, which is almost 3 orders of magnitude lower than what has been measured for marl [*Le Bouteiller et al.*, 2009]. For that reason, the grain size distribution of quarzite is assumed to remain constant during the experiment. Impacts between a marly pebble and a quartzite stone will then have no effect on the quarzite stone but might well affect the marly pebble.

[36] The concentration is assumed to be homogeneous at full transport stage, and is given by

$$C(r) = \frac{g(r) + q(r)}{V} \quad (14)$$

[37] V being the total volume of water in which the pebbles are moving in saltation, and $q(r)$ denoting the size distribution of quartzite material. By summing the contributions of particles of all sizes, the total number of impacts received by a particle of size r_1 during time dt is

$$n(r_1) = \frac{\pi \langle \tilde{u}^2 \rangle^{1/2}}{V} dt \int_0^\infty (r_1 + r_2)^2 (g(r_2) + q(r_2)) dr_2 \quad (15)$$

[38] So the collision frequency $\Phi(r_1)$ for a particle of size r_1 is

$$\phi(r_1) = \frac{\pi \langle \tilde{u}^2 \rangle^{1/2}}{V} \int_0^\infty (r_1 + r_2)^2 (g(r_2) + q(r_2)) dr_2 \quad (16)$$

[39] The collision frequency $\phi(r)$ is a nonlinear function of the grain size r, of the distribution g, and is evolving with time. It is then possible to express this collision frequency as a function of the mass x using equations (3) and (6). However, this is not detailed here since the numerical scheme is based on a size class discretization, as will be explained in section 6.

[40] Until now, the derivation has been performed for spherical particles. However, natural marly pebbles used for the experimental case study tend to be longer and more flat than spheres. The effective section for collision therefore depends on the orientation of the particles. For needle shape or flat particle, depending on the orientation of the main axis of the colliding particles, the effective section can be smaller or larger than what it would be for a sphere of similar mass. Let us consider an ellipsoidal particle of axis a_1, a_2 and a_3, with a_1 being the axis in the flow direction just before the collision. The volume of this particle is $4\pi a_1 a_2 a_3/3$, the equivalent radius is $(a_1 a_2 a_3)^{1/3}$ and the effective section in

Table 1. D90 and D50 Interpolated From Experimental Distributions

Time (min)	D90 (mm)	D50 (mm)	D90-D50 (mm)
0	42.5	26.4	16.1
10	34.5	19	15.5
20	31.3	13.2	18.1
30	28.5	<5	>23.5
60	21.5	<5	>16.5

Table 2. Statistical Analysis of Parameters Influence With the Logistic Regression

Parameter	Coefficient	Standard Error	p Value
Impact velocity	0.899	0.155	<0.001
Water saturation	0.082	0.284	>0.1
Number of previous impacts	0.074	0.088	>0.1
Mass	0.00048	0.00034	>0.1
Surface fissuration index	0.763	0.122	<0.001
Intercept	−5.710	0.830	<0.001

the sphere-like model would be $\pi(a_1a_2a_3)^{2/3}$, whereas the real effective section is πa_2a_3. The ratio θ between the reel effective section and the effective section of the sphere-like model is therefore given by

$$\theta = \left(\frac{a_2a_3}{a_1^2}\right)^{1/3} \tag{17}$$

[41] If a_1 is the main axis of the ellipsoidal particle, θ is lower than one whereas if a_1 is the smallest axis, θ is higher than one. In a turbulent flow in which the particles are likely to have all the possible orientations, we will then use as a first approach the approximation of the sphere-like model for the collision frequency.

[42] In previous experiments, *Hu and Hui* [1996] measured the trajectories of saltating particles and found that the distribution of particle velocities follows a Gaussian law where the fluctuations in velocity are proportional to the mean:

$$\left\langle \tilde{u}^2 \right\rangle^{1/2} = \sigma \bar{u} \qquad \sigma = 0.15 \tag{18}$$

[43] We assume a Gaussian law is appropriate for the experiments conducted here, but recognize that other distributions may be better suited for modeling transport in natural channels [*Lajeunesse et al.*, 2010]. In the experiments conducted here, the mean pebble velocity is 1.2 m/s, therefore the average fluctuation is easily estimated. For simplicity, the possible dependence of the velocity on the size of the particles is neglected here.

[44] In order to estimate the volume V occupied by the saltating particles, we used high-speed movies that were previously performed for 20–40 mm particles. According to the movie, most of these particles travel in the first 100 mm above the bed, some of them saltating a little higher. Marly pebbles being flatter, we eventually chose 150 mm as a correct approximation of the saltating height. Combining this with the surface of the annular flume leads to a value of the volume $V = 0.17$ m^3.

4.1.2. The Conditional Breakage Probability

[45] In order to estimate the breakage probability when a collision occurs, experimental measurements of impact breakage are performed. Marly pebbles from the river bed (of the Laval) are used. Pebbles are dropped in the air above a hard surface and fragmentation events are recorded. The influence of various factors is studied: initial mass m, impact velocity v, initial state of surface fracturation characterized by an index I, number of previous impacts, state of water saturation W. The surface fracturation index is used as a simplified indicator of the internal fractured structure of the material. It is equal to 0 for smooth pebbles, 1 for pebbles with surface discontinuities but without any apparent fracture, then 2, 3 or 4 for pebbles with apparent fractures of length smaller than 30%, between 30 and 60%, and longer than 60% of the size of the pebble, respectively. For more details about the experiments, see *Le Bouteiller et al.* [2010]. More than three hundred impacts are performed with mass ranging from 25 to 2000 g and impact velocity ranging from 1.2 to 6 m/s. Only two extreme states of water saturation were tested, with the pebbles being either left at ambient air or in the water during a few hours before the test. A statistical analysis is conducted in order to infer the probability of breakage and the relevant parameters influencing this probability. The analysis is performed on the variable "fragmentation" F using the logistic regression. F is a binary variable that can take only two values 0 or 1. The probability P that F takes the value 1 is assumed to be a function of the explanatory variables that are the mass m, velocity v, number of previous impacts N, fissuration index I and water saturation S. A generalized linear model is used, where $\ln(P/(1-P))$, also called the "logit" of P, depends linearly of the explanatory variables. The results of this analysis are presented in Table 2. According to this analysis, the mass, the number of previous impacts and the saturation are not statistically significant (p values > 0.1) so the conditional probability of breakage only depends on the impact velocity and on the surface fracturation index (p values < 0.001). The model for the conditional breakage probability P is therefore

$$\ln\frac{P}{1-P} = b_0 + b_1 v + b_2 I$$
$$P = \frac{e^{b_0+b_1v+b_2I}}{1+e^{b_0+b_1v+b_2I}}$$
$$b_0 = -5.3 \quad b_1 = 0.88 \quad b_2 = 0.79 \tag{19}$$

[46] It might be surprising to find that the mass is not a significant factor for the probability of rupture since several studies on other material [*Salman and Gorham*, 2000; *Andrews and Kim*, 1998] show that the size influences the breakage under impact. However, even if such a size effect existed in marl, the statistics indicate that the influence of the velocity and of the surface fracturation index is much more important. Equation (18) will then be used as a first approximation in the model, and the possible effects of the mass are neglected here. They will be discussed in section 7.

[47] This experiment was performed in the air, whereas it is used to describe impacts occurring in the water. Expected effects of water would be first a change in the mechanical properties of the saturated material, secondly a damping of the impact velocity. The impact velocities used in the experiment range from 1 to 6 m/s, therefore the model is valid for equivalent submerged impact velocities. Concerning the changes in mechanical properties, theories [*Alonso et al.*, 1990] predict that unsaturated materials have weaker mechanical properties. However, when testing both saturated and unsaturated pebbles, this effect has not been observed in the experiments, which does not mean that it is not present, but that its influence on the rupture is not statistically significant compared to the influence of the impact

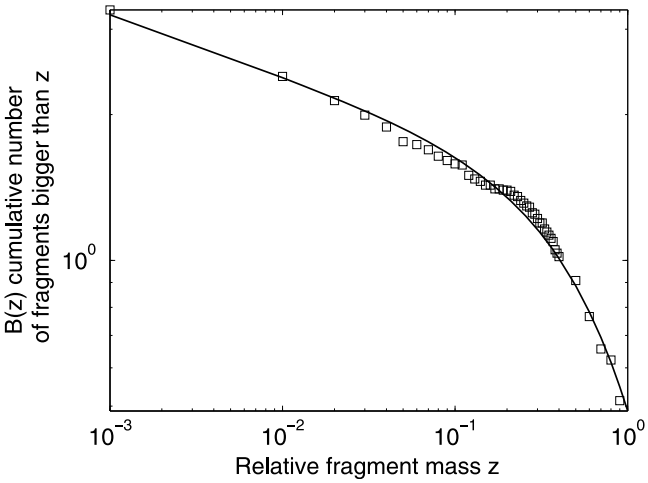

Figure 4. Cumulative number of fragments $B(z)$ as a function of the relative mass z. The squares are data from the rock dropping experiment, and the solid line is the model from equation (24).

velocity and of the surface state of fracturation. For that reason, the conditional rupture probability is assumed to be independent of the water saturation. Moreover, in the range of collision velocities that are involved and with gravel sizes larger than 5 mm, the collision Stokes numbers are much larger than the critical value of 105 for incipient viscous damping during collision [*Schmeeckle et al.*, 2001], suggesting that damping by viscous forces can be neglected. The possible effects of the water can therefore be neglected and the model that was determined from air experiments is valid for submersed impacts in the same range of velocities.

[48] The pebbles in the Laval river bed have surface indexes ranging from 0 to 4. However, the pebbles that were used in the study case experiment have been selected so that they can be transported to the laboratory, therefore there only are pebbles of indexes 0 or 1. The rupture probability, which increases with the surface index, is therefore likely to be lower in the flume experiment than in the real river. In the experimental conditions, the impact velocity is measured by the average velocity fluctuation according to equation (18). Eventually, the average resulting conditional breakage probability is $P = 0.005$.

4.1.3. The Resulting Breakage Probability

[49] Combining the value of P obtained from section 4.1.2 with equations (12) and (16), the general breakage frequency for the fragmentation process is

$$a_f(x,f) = P\psi(x) = P\phi(r) \tag{20}$$

4.2. The Daughter Distribution Function for Fragmentation

[50] The impact experiments on marly pebbles that is described in section 4.1.2 were also used to determine the daughter distribution. After each fragmentation event, all the fragments of mass larger than 1 g were collected and weighed. (Smaller fragments were not taken into account since the experimental setup did not allow to retrieve all of them properly). When fragmentation occurs, the number of fragments ranges from 2 to 11, with a mean value $\mu_N = 3.3$ and standard deviation $\sigma_N = 2.7$. Following *Diemer and Olson* [2002], a homogeneous formulation is assumed for the daughter distribution. It means that the expected number $p(x,y)\,dx$ of daughters of mass in the range $[x;\ x + dx]$ obtained from the breakage of a particle of mass y only depends on the relative mass $z = x/y$. This assumption is valid since neither the number of fragments nor the shape of the fragment size distribution appear to be influenced by the initial size of the pebble in the range of values that was tested (50 g to 2000 g). The number-based distribution b is therefore defined on [0; 1] so that

$$\begin{aligned} p(x,y)dx &= b(z)dz \\ p(x,y) &= \tfrac{1}{y}b(z) \end{aligned} \tag{21}$$

[51] The mass is conserved during each fragmentation event, therefore b must satisfy

$$\int_0^\infty zb(z)dz = 1 \tag{22}$$

[52] The mass distribution of the fragments is obtained by averaging the distributions over all the fragmentation events. As the measurements of the fracture distribution yield single events instead of the continuous distribution $b(z)$, it is more convenient to work with the total number of fragments $B(z)$ with relative masses equal to or larger than z.

$$B(z) = \int_z^\infty b(z')dz' \tag{23}$$

[53] Experimental and numerical studies about the fragmentation of brittle material [*Astrom et al.*, 2000; *Herrmann et al.*, 2006] have shown that the (retro) cumulative fragment-size distribution was of the form $B(z) \propto z^{-\tau}e^{-z}$. This distribution is also known as a tempered Pareto distribution. This expression was fitted to the data collected from the impact experiments by optimizing values of λ and τ and the following distribution was obtained:

$$B(z) = \mu_N \lambda z^{-\tau}e^{-z} \quad \lambda = 0.41 \quad \tau = 0.13 \qquad \left(R^2 = 0.97\right) \tag{24}$$

[54] Equation (24) is plotted in Figure 4 together with the experimental values of the distribution.

[55] The fitted model reproduces properly the data from the experiments, except for the very small sizes and for the very large sizes. First, it diverges when $z \to 0$, whereas it should reach a maximum value equal to the average number of fragments μ_N. Moreover, it does not reach zero for $z = 1$, whereas it is physically impossible to get a daughter particle with mass larger than the initial particle. For these reasons, the validity of equation (24) is restrained to $z \in [z_0;\ 1]$,

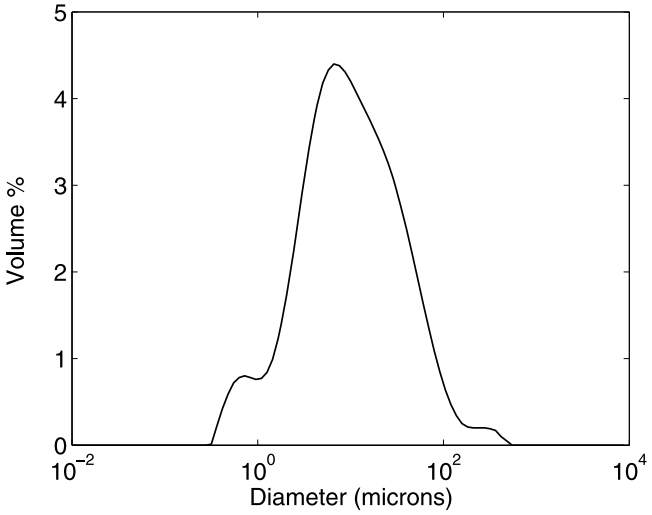

Figure 5. Grain-size distribution of the suspension formed measured with a laser device.

denoting z_0 the value for which $\lambda z_0^{-\tau} e^{-z0} = 1$, $z_0 \approx 0.001$. The model is then modified as follows:

$$B^*(z) = \mu_N \text{ for } z < z_0$$
$$B^*(z) = \mu_N \lambda z^{-\tau} e^{-z} \text{ for } z \in [z_0; 1[$$
$$B^*(z) = 0 \text{ for } z = 1 \quad (25)$$

[56] Eventually, the daughter distribution for fragmentation p_f is obtained by deriving and rescaling B as follows:

$$p_f(x,y) = 0 \text{ for } \frac{x}{y} < z_0$$
$$p_f(x,y) = -\frac{1}{y}\frac{dB^*}{dz} \text{ for } z \in [z_0; 1[$$
$$p_f(x,y) = 0 \text{ for } z = 1 \quad (26)$$

4.3. The Daughter Distribution Function for Abrasion

[57] In the present study, abrasion is modeled as a binary rupture event in which a mother particle is broken into one very small particle and one almost-unchanged particle. Since it is a surface process, it is assumed that the mass ϵ of the small particle is independent of the size of the mother particle. The daughter distribution p_a can therefore be written using the Dirac function δ:

$$p_a(x) = \delta(x - \epsilon) + \delta(x - y + \epsilon) \quad (27)$$

[58] Grain-size measurements with a laser diffraction device are performed on the suspension resulting from the abrasion experiments in order to determine the average size of the small particle produced by abrasion. The resulting spectra is plotted in Figure 5. Since the discretization scheme adopted later will not allow to distinguish the exact sizes, the mean value can be simply used to characterize the distribution of sizes for suspended sediment. The mean value of the diameter is found to be 7 microns, which corresponds to a mass $\epsilon = 4.7 \cdot 10^{-10}$ g.

4.4. The Breakage Probability for Abrasion

[59] Sternberg's law (see equation (2)) is used to quantify abrasion through a unique fining coefficient α, which represents (at first order) the percentage of mass that is removed from a grain after traveling a unit distance. For a particle of mass x, in kg, the amount of mass removed by abrasion according to Sternberg's law has to be equal to the frequency of abrasion events multiplied by the mass of small abraded particles ϵ.

$$\alpha \bar{u} x = a_a(x)\epsilon$$
$$a_a(x) = \frac{\alpha \bar{u}}{\epsilon} x \quad (28)$$

[60] Equation (28) shows that the abrasion frequency has to be proportional to the mass in order to respect the Sternberg's law. An equivalent description would be to consider that abrasion events are not binary ruptures and produce a number of fine particles that is proportional to the size of the initial particle, which would lead to a constant abrasion frequency. This description may seem physically more realistic but is more complex to implement numerically so the mathematically equivalent description of binary ruptures is preferred.

[61] In order to isolate the effect of abrasion, a separate set of experiments was performed on five marly pebbles using a smaller flume similar to the main flume. Transport conditions in the small device are less intense than in the big one, thus no fragmentation was observed, and the only process responsible for size/mass reduction is abrasion. Sternberg's degradation coefficient for marls, α, which is extracted from these experiments, is therefore a real abrasion coefficient. The measurements from the small flume give an abrasion coefficient of α = 18%/km. Similar experiments have been performed in both small and large flumes with another type of marl which is more resistant and less prone to fragmentation. The resulting abrasion coefficients, which account only for abrasion, are 4.6 and 8.6%/km in the small and large flumes, respectively. They reflect the differences in size and transport conditions between the two flumes. The scaling correction factor of 1.9 is therefore used for our experiments, providing an estimate of the abrasion coefficient in the large flume of 34%/km.

5. Simulation Methods

[62] The model is fully determined by equations (20), (26), (27) and (28).

[63] For simulation, a size class discretization is used. Class i is defined as the assembly of particles of mass/volume within the range $[x_{i-1}, xi]$, with

$$x_0 = 0$$
$$x_1 = x_{\min}$$
$$x_{i+1} = R x_i \text{ for } i \geq 1 \quad (29)$$

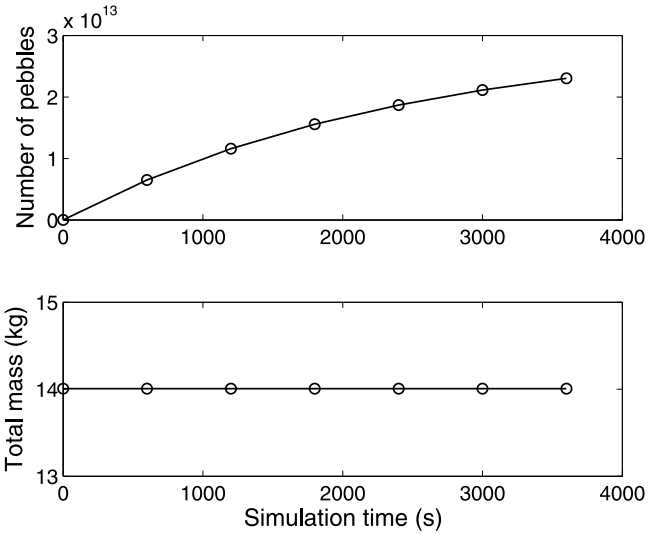

Figure 6. Evolution of the zeroth and first moments of the distribution for an abrasion simulation of 1 h.

[64] The geometrical parameter R regulates the spatial resolution, it is fixed to 1.5. The volume is expressed in cubic millimeters. In the study case, pebbles of diameter up to 60 mm are used, so 35 classes are used.

[65] The number of particles f_i inside a given size class i is therefore given by

$$f_i(t) = \int_{x_{i-1}}^{x_i} f(x,t)dx \;\forall i \tag{30}$$

[66] Eventually, the partial differential equation (10) is transformed into a system of simple differential discretized equations for all the classes where $i > 1$:

$$\begin{aligned}\frac{d}{dt}f_i(t) &= \sum_{j=i}^{\infty}\left(a_{a,j}p_{a,ij}f_j(t) + a_{f,j}p_{f,ij}f_j(t)\right) \\ &\quad - a_{a,i}f_i(t) - a_{f,i}f_i(t) \text{ for } i > 1 \\ &= \sum_{j=i}^{\infty}\left(a_{a,j}p_{a,ij}f_j(t) + a_{f,j}p_{f,ij}f_j(t)\right) \text{ for } i = 1\end{aligned} \tag{31}$$

[67] For the class $i = 1$, the two last terms disappear since no breakage either by fragmentation or by abrasion is allowed. $a_{a,i}$, $a_{f,i}$, are the discretized forms of the breakage frequencies in class i, and $p_{a,ij}$ and $p_{f,ij}$ are the size distributions of fragments of size i coming from the breakage of a particle of size j. The procedure for inferring these functions from the continuous form can be obtained in the work by *Hill and Ng* [1995].

[68] A major problem due to the size class discretization is the preservation of the mass: with the basic discretized model of equation (31), a particle from class i which is subject to abrasion should produce a particle in the class i-1 and another one in class $i = 1$ of mass ϵ. However, most of the time, the removal of ϵ from the mass of the initial real particle will not change its mass enough for it to shift into a smaller size class. The same problem arises for the fragmentation description. In order to preserve the mass, probability birth and death functions are used following *Hill and Ng* [1995]. For instance, with this correction, a particle of class i which is subject to abrasion will move to class i-1 only with a probability smaller than 1 which depends on its size and on the width of the size class.

[69] The following procedure is used for the simulation.

[70] 1. Initial distribution is provided for marl as well as quartzite material.

[71] 2. Mass distribution is transformed into a number-based distribution.

[72] 3. Functions for the breakage frequency, the daughter distributions, and birth and death correction, are provided as matrix.

[73] 4. The system of differential equations (31) is solved with an explicit Runge-Kutta method.

6. Results

[74] The initial experimental number-based volume distribution that is shown in Figure 2 is used as an initial condition for the model. It is interpolated on the model size discretization according to a lognormal law. The model is first run with one-process loadings: run 1 with only abrasion and run 2 with only fragmentation. Eventually, the model is run with the two processes. For each run, the total simulation time is 60 min, which is similar to the duration of the experiments.

6.1. Results From the Abrasion Simulation

[75] For the abrasion run, the evolution of the zeroth and first moments is plotted in Figure 6. The mass is conserved during the simulation, which means that the correction procedure with birth and death functions that was used works properly. The number of particle increases with time, all the newly created particles being in the smallest size class, and the number of small particles produced by abrasion after 1 h is $2.4 \cdot 10^{13}$, corresponding to the number of abrasion events that were calculated by the model. The evolution of the number of small particles $n_\epsilon(t)$ follows a law which is complementary to the Sternberg abrasion law for the mass of the coarse material:

$$n_\epsilon(t) = \frac{M}{\epsilon}\left(1 - \exp\left(-\frac{\alpha}{\bar{u}}t\right)\right) \qquad \left(R^2 = 1\right) \tag{32}$$

[76] The evolution of the cumulative mass distribution is plotted in Figure 7. Abrasion is responsible for a shift in the mass distribution toward the small sizes mainly due to the production of fine particles. After 1 h, fine particles (i.e., particles of mass smaller than x_{min}) represent 77% of the total mass. On the other hand, the coarse part of the distribution is not much modified during the simulation. D90 and D50 values are interpolated from the cumulated distributions and presented in Table 3. The difference between these two values, D90-D50, is used as an indicator of the dispersion within the largest size classes, and is represented in Figure 8. In the abrasion simulation, this difference increases with time. Indeed, the D50 decreases faster than the D90, which lead to a spreading of the right part of the distribution.

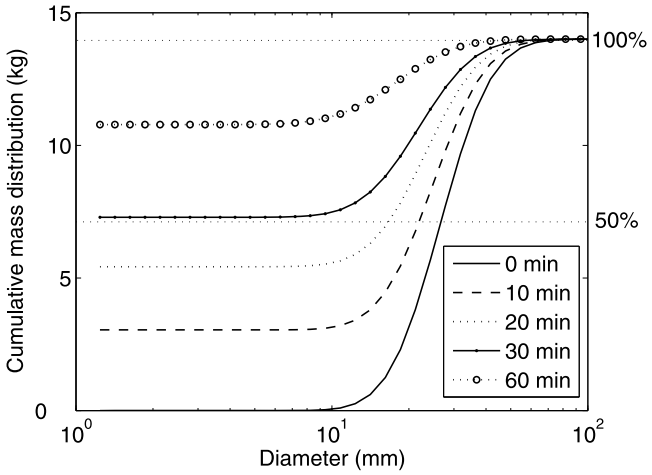

Figure 7. Grain-size distributions from the model running with only abrasion. The fraction of the total mass is indicated on the right axis.

[77] For a quantitative comparison with experimental data, the predicted distributions are interpolated at the values of diameter corresponding to the sieves used in the experiments. The predicted values of the cumulative mass at various times are then compared to the experimental values as shown in Figure 9. A global correlation analysis between all the predicted and observed values provides a coefficient $R^2 = 0.98$ and the mean deviation between predicted and observed values is 5%.

6.2. Results From the Fragmentation Simulation

[78] For the fragmentation run, the evolution of the zeroth and first moments is plotted in Figure 10. As for the abrasion, the total mass is conserved. With fragmentation, the number of particles increases rapidly at the beginning of the simulation as the increasing number of particles provide more collisions, but then slows down. After a 1 h run, the number of pebbles reaches $4.2 \cdot 10^9$.

Table 3. D90 and D50 Interpolated From the Abrasion Simulation

Time (min)	D90 (mm)	D50 (mm)	D90-D50 (mm)
0	42.5	26.4	16.1
10	38.4	21.7	16.7
20	34.2	16.3	17.9
30	30.3	<1	>29.3
60	19.2	<1	>18.2

[79] The evolution of the cumulative mass distribution is plotted in Figure 11. The degradation by fragmentation is initially slow during the first minutes then accelerates so that after 7 min, all the particles are in the two smallest classes and the distribution does not evolve anymore. The number of particles is still increasing which indicates that some fragmentation events still occur within the second smallest class but most of the resulting fragments stay in this class. This accelerating degradation can be predicted from equations (20) and (16), according to which the collision frequency is roughly the product of the squared radius of the particles r^2 by the number of particles. Mass conservation implies that the number of particles evolves as r^{-3}. The collision frequency is therefore proportional to r^{-1} and increases as the particle radiuses decrease.

[80] As for abrasion, fragmentation produces a shift of the mass distribution toward the small sizes. However, contrary to what was observed for abrasion, the mass in the smallest size class only represents 0.01% of the total mass after a 1 h run. Not many very fine particles are produced and most of the small particles produced by fragmentation actually stay in the second smallest size class. The major changes in the fragmentation simulation occur in the largest size classes, the largest nonempty size class becoming smaller as the largest particles disappear. The D90 and D50 values are interpolated from the cumulated distributions and presented in Table 4. In the fragmentation simulation, the difference D90-D50 decreases with time, as shown in Figure 8. This denotes a shrinkage of the right part of the distribution.

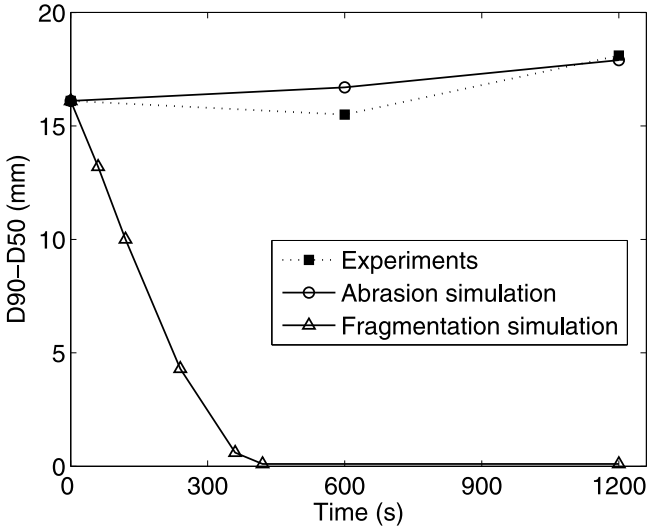

Figure 8. Evolution of the difference D90-D50 in the experiments and in the abrasion and fragmentation simulations, during the first 20 min.

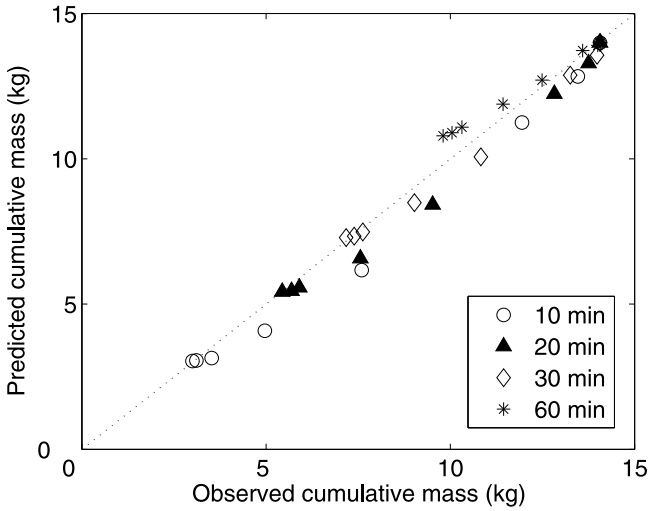

Figure 9. Predicted values for the abrasion simulation versus experimental values of the cumulative mass at various times.

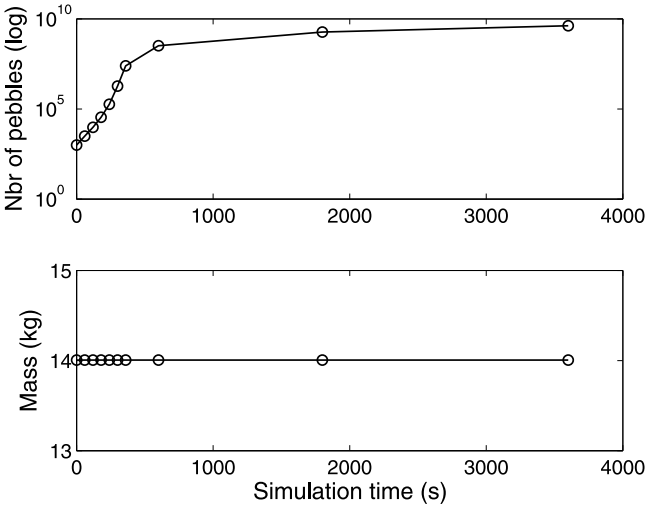

Figure 10. Evolution of the zeroth and first moments of the distribution for a fragmentation simulation of 1 h.

[81] The predicted cumulative mass distributions are interpolated at the sieve diameters at the simulation times corresponding to the experiment. The comparison of the predicted values versus the observed ones is plotted in Figure 12. After 10 min, which is the first time step for which experimental data is available, the predicted values are all 14 kg, which means that all the mass has already been degraded into particles smaller than the smallest sieve (5 mm). This shows that the fragmentation alone is not able to explain the observed distributions for a time scale of 10 to 60 min. Indeed, the experimental distributions do not present an accelerating degradation as predicted by the fragmentation model (see Figure 11), so the fragmentation in the experiment is slowed down compared to the model of equation (20).

7. Discussion

[82] Comparing the predictions of the model for one-process or two-process simulations to the experimental grain size distributions provides new insights into what happens during the transport.

Table 4. D90 and D50 Interpolated From the Fragmentation Simulation

Time (min)	D90 (mm)	D50 (mm)	D90-D50 (mm)
0	42.5	26.4	16.1
1	36	22.9	13.2
2	28.2	18.2	10
4	11.8	7.5	4.3
6	2	1.4	0.6

7.1. Abrasion and Fragmentation Processes Are Both Involved

[83] In Figure 2, two main features of the experimental distribution are to be noted. First, the particles of the smallest class, which are the particles of size lower than 5 mm, represent an increasing proportion of the total mass, reaching 70% after a 1 h experiment. This first feature is not reproduced by the fragmentation simulation and corresponds to the production of fine particles through the abrasion process, as it appears clearly in the abrasion simulation.

[84] Secondly, there are also some changes in the coarse part of the distribution, which are especially accounted for by the decrease of the D90 (see Table 1). The difference D90-D50 is plotted in Figure 8 with the values interpolated from experimental data and from the simulations with abrasion or fragmentation. In the first 10 min of the experiment, the D90 decreases faster than the D50, denoting a shrinkage of the coarse part of the distribution. However, this tendency seems to invert afterward. The shrinking pattern in the largest size classes is characteristic of the fragmentation process, for which the difference D90-D50 decreases rapidly, whereas it increases for the abrasion simulation.

[85] The abrasion simulation reproduces properly the first feature, and provides a quantitatively correct prediction of the production of fine particles. Indeed, the amount of fine

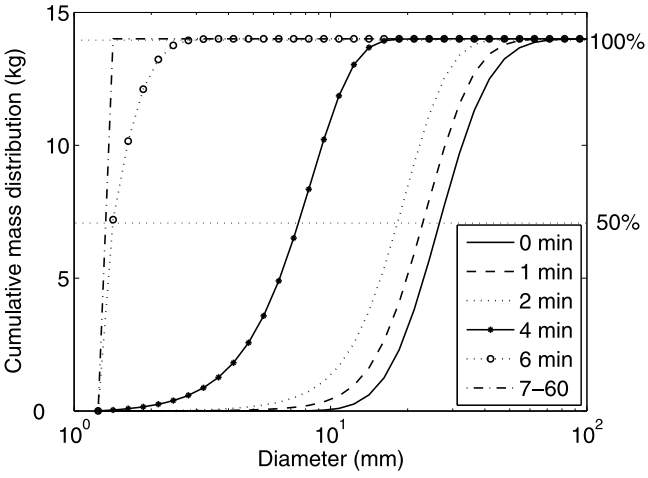

Figure 11. Grain-size distributions from the model running with only fragmentation. The fraction of the total mass is indicated on the right axis.

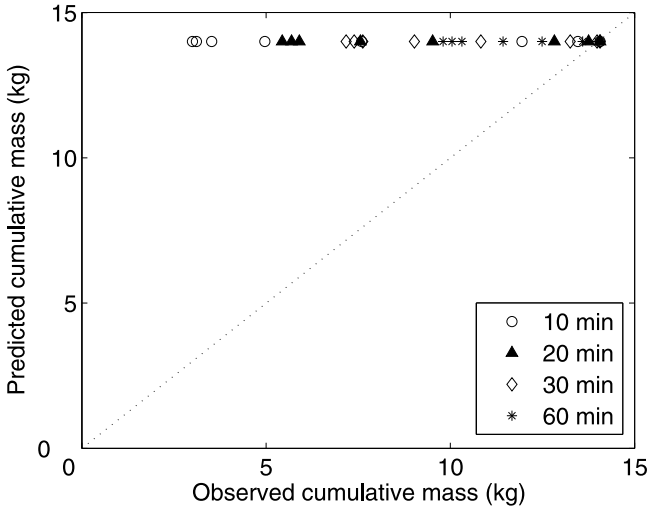

Figure 12. Predicted values for the fragmentation simulation versus experimental values of the cumulative mass at various times.

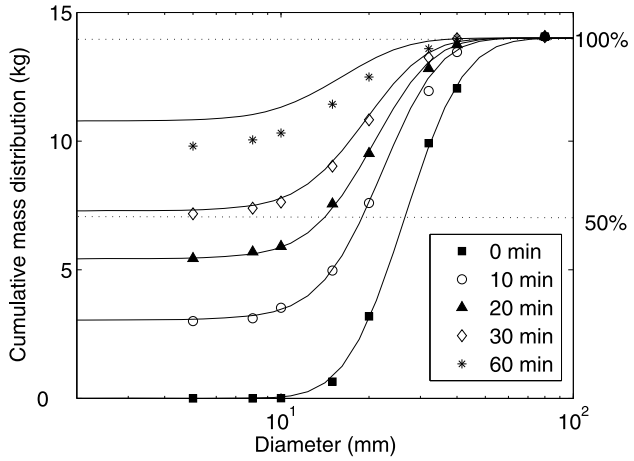

Figure 13. Experimental and predicted distributions. The simulation is run with abrasion and time-dependent fragmentation with t_0 = 70 s. The black lines represent the predictions of the model. The fraction of the total mass is indicated on the right axis.

particles at the end of the experiment is 70% whereas the abrasion simulation predicts a value of 77%. The small difference is probably due to the estimation of the scaling coefficient between the small and large flume. Moreover, the overall estimation of the abrasion simulation is quite good since the mean deviation for the predictions of the cumulative mass is 5%. However, the abrasion simulation fails in modifying the proportion of particles in the upper classes. On the other hand, the fragmentation simulation is appropriate to model the changes in the upper classes at least during the first steps of the experiments, but does not produce as many fine particles as observed in the experiments. Combining the effects of abrasion and fragmentation is therefore necessary to explain what is observed in the experiments.

[86] The comparison of one-process simulated and experimental distributions suggests that abrasion and fragmentation are both involved in the experimental degradation. The specific shape of the grain-size distributions is therefore a signature of the mechanisms at stake in the degradation.

7.2. Fragmentation Is a Time-Dependent Process

[87] Results from the fragmentation simulation have shown that the number of particles increases very fast (see Figure 10). The resulting number of coarse particles after 1 h is therefore much higher than what was observed in the experiments. At the same time, D90 values decrease much faster in the simulation than in the experiments (see Tables 4 and 1 and Figure 8). Moreover, in the experiments, the difference D90-D50 first decreases, denoting a fragmentation-like shrinkage, then increases, as if fragmentation become less important and its effects are hidden by abrasion effects. These observations suggest that the fragmentation process becomes less and less important during the experiment. The fragmentation "efficiency" is decreasing.

[88] This could reflect an evolution of the mechanical properties of the daughter fragments relatively to their initial parent pebble. Indeed, marly material has a very heterogeneous structure which is characterized by the existence of a fracture net in the rock. It is mostly probable that at the beginning of the experiment, fragmentation occurs along preexisting internal fractures, so that after a while, the remaining pebbles are stronger and the fragmentation efficiency is damped. In average, the population become stronger once the weakest individuals have been broken. Such process was also observed by *Attal and Lavé* [2009] for limestone pebbles. In their experiments, if the same material was reused, they found lower fragment production rates in the second experiments than in the first ones, because splitting and breaking primarily occurs on discrete weakness zones within the pebbles (bedding plane, fracture, tension gash).

[89] Alternatively, this could also be explained by some intrinsic size dependency of fragmentation although our free fall experiments (see section 4.1.2) do not suggest that large particles are more prone to break than small ones. Hertz theory for elastic deformable spheres predicts that the pressure in the contact zone due to an impact is independent of the size [*Johnson*, 1985]. The rupture occurs when the stress associated with this pressure reaches the tensile strength, which can depend on the size. *Lobo-Guerrero and Vallejo* [2006] showed that the influence of the sample size on the tensile strength is controlled by the Weibull modulus, which is a parameter of the distribution of local strength inside the material. This parameter depends on the material, therefore the influence of the size is not the same in every material. If there is a large variability of strength within a rock, it will be much more probable to find a weak zone in a big sample than in a small one. For marl, which has a very heterogeneous material, one should expect a low value of the Weibull modulus corresponding to a great variability of strength. Therefore the effect of size on the breakage should not be negligible. Further work would therefore be necessary to quantify this possible size dependence and integrate this effect into the present model.

[90] Here, for simplicity, the time dependence of the fragmentation efficiency will be introduced through the use of a characteristic time scale t_0:

$$a_f^* = \exp\left(\frac{t}{t_0}\right) \tag{33}$$

[91] t is the transport duration and t_0 is the time scale of the decrease of fragmentation efficiency. Several simulations with values of t_0 ranging from 10 to 200 s have been performed and show that the best correlation is obtained for a value of t_0 = 70 s. Fragmentation therefore occurs mostly during the first minute of the experiment. Since the grain size does not change much during one minute, the hypothesis of a size dependence of the fragmentation probability cannot explain alone this decrease. The first hypothesis, according to which grains become stronger in average once the weakest pebbles are broken, is more consistent with a short time scale, and therefore seems to be a better explanation.

[92] A new 1 h simulation is conducted with abrasion and time-dependent fragmentation with t_0 = 70 s. The results are plotted in Figure 13 next to the experimental data. The model predictions are very similar to the experimental

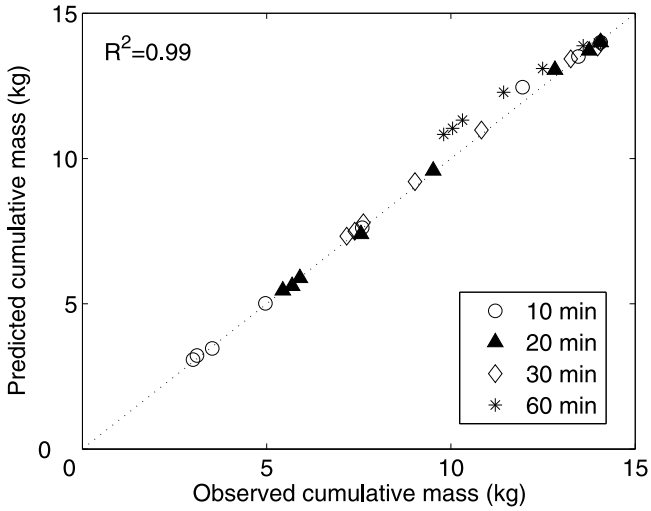

Figure 14. Predicted values versus experimental values of the cumulative mass at various times, for the simulation with abrasion and time-dependent fragmentation.

distributions, although it overestimates by 7% the production of fine particles by abrasion after 1 h. A correlation analysis is performed according to the procedure that was described in section 6.1. The predicted values are plotted versus the observed values of cumulative mass in Figure 14. The correlation analysis provides a global correlation coefficient R^2 = 0.99 and the mean deviation between the predicted and observed values is 1.2%.

[93] Taking into account the effects of a time-dependent fragmentation process therefore improves the abrasion model, for which the deviation was 5%.

7.3. Coupled Effects

[94] In section 2, it was assumed that abrasion and fragmentation mechanisms acted separately on the pebbles and that their effects could be simply added. However, this is questionable when taking the shape of the grains into account. Indeed abrasion and fragmentation have opposite effects on the shape of pebbles, and some feedback may occur through the shape. Abrasion tends to make particles rounder whereas fragmentation produces angular stones [*Goede*, 1975].

[95] It has long been noticed that angular pebbles were more sensitive to abrasion processes [*Kuenen*, 1956], and fragmentation does produce angular shapes. Abrasion should then be enhanced by fragmentation events. On the other hand, there is no clear feedback of the shape on fragmentation.

[96] Eventually, there seems to be a competition between abrasion and fragmentation processes for the control of the shape. As was explained in section 7.2, fragmentation efficiency decreases progressively during the experiments, therefore abrasion effects become dominant. This is confirmed by our observations: indeed, at the end of the experiments, the pebbles are much rounder than at the beginning.

[97] An approach based on the analysis on the pebble shape distribution would be useful to understand the coupling effects between abrasion and fragmentation processes. For instance, one could consider the proportion of round pebbles versus angular fragments, or a continuous shape distribution, by characterizing the distribution of curvatures along the pebbles contour as proposed by *Durian et al.* [2007]. Following *Hill* [2004], the shape distribution could then be integrated into the Population Balance Equation framework by developing joint probability distribution accounting for both the shape and the size.

8. Conclusion

[98] A model based on the physical and statistical description of abrasion and fragmentation processes was proposed and applied to simulate the degradation of marly sediment in an experimental flow. The model reproduces the effects of abrasion and fragmentation on the grain size distribution. Comparison with experimental data shows the following.

[99] 1. Both mechanisms are involved in the experiments and it is necessary to take fragmentation and abrasion into account to explain the observed changes in the size distribution.

[100] 2. Fragmentation efficiency decreases during the experiment. Indeed, the weakest stones with preexisting fractures are broken first, then the breakage process slows down when only the strongest ones remain. A characteristic time of 70 s accounts properly for the observations.

[101] 3. Fragmentation and abrasion have opposite effects on the shape, and there is a feedback of the shape on the abrasion mechanism. With the decrease of fragmentation efficiency, abrasion effects dominate and lead to rounder pebbles.

[102] This model has been first applied to the degradation of pebbles in an experimental flow, and show promising results, for qualitative as well as quantitative aspects. Next step will be to apply it to a real river. This will require to describe in a similar framework the other processes that affect sediment size in a real river, such as selective transport, side input from the hillslopes or sediment weathering between the floods. Such a model will then be a useful tool for an inverse analysis. By looking at the grain-size distributions of bed load sediments, and comparing them to the model predictions, one will be able to infer some information about the physical processes that have resulted into such distributions.

[103] This paper introduces a new framework for the study of transport phenomena associated with a degradation of the material. It also proposes a methodology for determining the elementary functions of the model. This methodology includes impact experiments, abrasion experiments and a grain-size measurement of the fine particles produced by abrasion. Here, the model is developed and applied to marly sediment transport in a stream, but the methodology is adaptable to other materials and breakage mechanisms, and the framework that was developed might help for dealing with any kind of transport associated with a degradation of the material, such as rock or snow avalanches, drifting snow, debris flows or pyroclastic flows.

Notation

a breakage frequency in a general case (s^{-1}).
a_a abrasion breakage frequency (s^{-1}).
a_f fragmentation breakage frequency (s^{-1}).

B cumulative homogeneous fragment size distribution.
B^* corrected model for the cumulative fragment size distribution.
b homogeneous fragment size distribution.
b_0 b_1 b_2 fitted parameters of the rupture probability law.
C number-based particle concentration.
D particle diameter (m).
D_0 initial particle diameter (m).
$f(x, t)$ number-based density function, as a function of the particle mass x.
F binary variable for the fragmentation under impact.
$g(D, t)$ number-based density function, as a function of the particle diameter D.
I surface fissuration index.
l traveled distance (m).
M total mass of the population (kg).
m mass of one pebble (kg).
$N(t)$ total number of particles at time t.
N_f average number of fragments in a fragmentation event.
$n(r)$ number of impacts on one particle of radius r during time dt (s^{-1}).
$n_r(r_1, r_2)$ number of impacts on one particle of radius r_1 from particles of radius r_2.
n_ϵ number of fine particles in the smallest class.
P conditional breakage probability.
p daughter distribution in a general case.
p_a daughter distribution for abrasion.
p_f daughter distribution for fragmentation.
$q(r)$ grain-size distribution of the quartzite material.
r particle radius (m).
R size class discretization parameter.
t time (s).
t_0 characteristic time for the decrease of fragmentation efficiency (s).
$\bar{u}$ average particle velocity ($m.s^{-1}$).
$\tilde{u}$ particle velocity fluctuation ($m.s^{-1}$).
V total water volume (m^3).
v impact velocity ($m.s^{-1}$).
W water saturation level in a pebble.
x particle mass (kg).
$x_{\min}$ limit mass under which no breakage (kg).
y mother particle mass (kg).
z relative fragment mass.
z_0 parameter of the fragment size distribution.
α Sternberg's abrasion coefficient in mass (m^{-1}).
β Sternberg's abrasion coefficient in diameter (m^{-1}).
δ Dirac distribution.
ϵ mass of the small particle removed by abrasion (kg).
θ ratio of the real effective surface of an ellipsoidal particle to the sphere-like model effective surface.
λ parameter of the fitted fragment size distribution.
μ_N average number of fragments in fragmentation.
ρ material density (kg/m^3).
σ relative velocity fluctuation.
σ_N standard deviation of the number of fragments in fragmentation.
τ parameter of the fitted fragment size distribution.
$\phi(r)$ collision frequency for a particle of radius r (assembly of spheres).
$\phi_c(r)$ collision frequency for a particle of radius r (assembly of nonspherical particles).
$\psi(x)$ collision frequency for a particle of mass x (s^{-1}).

[104] **Acknowledgments.** The authors thank the STEVAL team from the *Laboratoire Environnement et Minéralurgie* as well as Master student C. Lepiouf for their help in the realization of the experiments. Careful reviews from N. Bradley, M. Schmeekle, J. Pitlick, and an anonymous referee helped us improve the paper.

References

Alonso, E. E., A. Gens, and A. Josa (1990), A constitutive model for partially saturated soils, *Geotechnique*, *40*(3), 405–430.
Andrews, E. W., and K. S. Kim (1998), Threshold conditions for dynamic fragmentation of ceramic particles, *Mech. Mater.*, *29*(3–4), 161–180.
Astrom, J. A., B. L. Holian, and J. Timonen (2000), Universality in fragmentation, *Phys. Rev. Lett.*, *84*(14), 3061–3064.
Attal, M., and J. Lavé (2009), Pebble abrasion during fluvial transport: Experimental results and implications for the evolution of sediment load along rivers, *J. Geophys. Res.*, *114*, F04023, doi:10.1029/2009JF001328.
Attal, M., J. Lavé, and J.-P. Masson (2006), New facility to study river abrasion processes, *J. Hydraul. Eng.*, *132*(6), 624–628.
Brewer, P. A., and J. Lewin (1993), In-transport modification of alluvial sediment: Field evidence and laboratory experiments, in *Alluvial Sedimentation*, edited by M. Marzo and C. Puigdefábregas, pp. 23–35, Blackwell Sci., Oxford, U. K.
Brierley, G. J., and E. J. Hickin (1985), The downstream gradation of particle sizes in the Squamish River, British Columbia, *Earth Surf. Processes Landforms*, *10*(6), 597–606.
Chatanantavet, P., G. Parker, E. Lajeunesse, P. Planton, and P. Valla (2008), Physically-based model of downstream fining in bedrock streams with side input and verification with field data, in *River, Coastal and Estuarine Morphodynamics: RCEM 2007*, edited by C. M. Dohmen-Janssen and S. J. M. H. Hulscher, pp. 571–579, Taylor and Francis, London.
Diemer, R. B., and J. H. Olson (2002), A moment methodology for coagulation and breakage problems: Part 3—Generalized daughter distribution functions, *Chem. Eng. Sci.*, *57*(19), 4187–4198.
Durian, D. J., H. Bideaud, P. Duringer, A. P. Schröder, and C. M. Marques (2007), Shape and erosion of pebbles, *Phys. Rev. E*, *75*(2), 021301, doi:10.1103/PhysRevE.75.021301.
Frings, R. M. (2008), Downstream fining in large sand-bed rivers, *Earth Sci. Rev.*, *87*(1–2), 39–60.
Goede, A. (1975), Downstream changes in shape in the pebble morphometry of the Tambo River, eastern Victoria, *J. Sediment. Petrol.*, *45*(3), 704–718.
Herrmann, H. J., F. K. Wittel, and F. Kun (2006), Fragmentation, *Physica A*, *371*(1), 59–66.
Hill, P. J. (2004), Statistics of multiple particle breakage accounting for particle shape, *AIChE J.*, *50*(5), 937–952.
Hill, P. J., and K. M. Ng (1995), New discretization procedure for the breakage equation, *AIChE J.*, *41*(5), 1204–1216.
Hu, C., and Y. Hui (1996), Bed-load transport. II: Stochastic characteristics, *J. Hydraul. Eng.*, *122*(5), 255–261.
Iveson, S. M., J. D. Litster, K. Hapgood, and B. J. Ennis (2001), Nucleation, growth and breakage phenomena in agitated wet granulation processes: A review, *Powder Technol.*, *117*(1), 3–39.
Johnson, K. L. (1985), *Contact Mechanics*, Cambridge Univ. Press, Cambridge, U. K.
Kendall, K. (1978), The impossibility of comminuting small particles by compression, *Nature*, *272*(5655), 710–711.
Kodama, Y. (1994a), Downstream changes in the lithology and grain size of fluvial gravels, the Watarase River, Japan: Evidence of the role of abrasion in downstream fining, *J. Sediment. Res., Sect. A*, *64*(1), 68–75.
Kodama, Y. (1994b), Experimental study of abrasion and its role in producing downstream fining in gravel-bed rivers, *J. Sediment. Res., Sect. A*, *64*(1), 76–85.
Kuenen, P. H. (1956), Experimental abrasion of pebbles: 2. Rolling by currents, *J. Geol.*, *64*, 336–368.
Lajeunesse, E., L. Malverti, and F. Charru (2010), Bedload transport in turbulent flow at the grain scale: Experiments and modeling, *J. Geophys. Res.*, *115*, F04001, doi:10.1029/2009JF001628.
Le Bouteiller, C., F. Naaim, N. Mathys, and J. Lavé (2009), Degradation processes in marly sediment transport, in *RCEM 2009*, edited by L. P. Vionet et al., pp. 257–261, CRC Press, Leiden, Netherlands.

Le Bouteiller, C., C. Guironnet, F. Naaim, and N. Mathys (2010), Experimental study of marl fragmentation, paper presented at EPFL Doctoral Conference in Mechanics, Am. Inst. Phys., Lausanne, Switzerland.

Lewin, J., and P. A. Brewer (2002), Laboratory simulation of clast abrasion, *Earth Surf. Processes Landforms*, *27*(2), 145–164.

Lobo-Guerrero, S., and L. E. Vallejo (2006), Application of Weibull statistics to the tensile strength of rock aggregates, *J. Geotech. Geoenviron. Eng.*, *132*(6), 786–790.

Mathys, N., S. Brochot, M. Meunier, and D. Richard (2003), Erosion quantification in the small marly experimental catchments of Draix (Alpes de Haute Provence, France): Calibration of the ETC rainfall-runoff-erosion model, *Catena*, *50*(2–4), 527–548.

Parker, G. (1991), Selective sorting and abrasion of river gravel: 1. Theory, *J. Hydraul. Eng.*, *117*(2), 131–147.

Parker, G. (2008), Comminution as a mechanism for downstream fining in rivers: Formulation, in *River Flow 2008*, edited by M. Altinakar et al., pp. 1323–1330, Kubaba Congr. Dep. and Travel Serv., Ankara.

Ramkrishna, D. (1985), The status of population balances, *Rev. Chem. Eng.*, *3*(1), 49–95.

Salman, A. D., and D. A. Gorham (2000), The fracture of glass spheres, *Powder Technol.*, *107*(1–2), 179–185.

Schmeeckle, M. W., J. M. Nelson, J. Pitlick, and J. P. Bennett (2001), Interparticle collision of natural sediment grains in water, *Water Resour. Res.*, *37*(9), 2377–2397.

Sternberg, H. (1875), Untersuchungen uber Langen-und Querprofil geschiebefuhrender Flusse, *Z. Bauwes.*, *25*, 486–506.

J. Lavé, CRPG-CNRS, 15 Rue de Notre-Dame des Pauvres, F-54501 Vandoeuvre-lès-Nancy, France.

C. Le Bouteiller, N. Mathys, and F. Naaim-Bouvet, Cemagref ETNA, 2 Rue de la Papeterie, BP 76, F-38402 St. Martin d'Heres, Grenoble CEDEX, France. (caroline.le-bouteiller@m4x.org)